Eye (2021) 35:2855–2863
https://doi.org/10.1038/s41433-020-01332-w

The ROYAL COLLEGE of OPHTHALMOLOGISTS

ARTICLE

# Clinical features of ocular toxocariasis: a comparison between ultra-wide-field and conventional camera imaging

Songshan Li[1] · Limei Sun[1] · Chengxi Liu[2] · Weiqing Wang[1] · Sijian Huang[1] · Ting Zhang[1] · Chonglin Chen[1] · Zhirong Wang[1] · Liming Cao[1] · Xiaoling Luo[1] · Bilin Yu[1] · Xiaoyan Ding[1]

Received: 28 July 2020 / Revised: 20 October 2020 / Accepted: 17 November 2020 / Published online: 3 December 2020


## Abstract

**Purpose** The purpose of this study is to compare the lesion detection rates of ocular toxocariasis (OT) between ultra-wide-field scanning laser ophthalmoscopy (UWF-SLO) and conventional fundus photography (CFP), and to evaluate the potential diagnostic ability of UWF-SLO in OT.

**Methods** A total of 56 patients with serological/immunological confirmed unilateral OT were enrolled. The presence of OT characteristic features included the posterior granuloma (postG), peripheral granuloma (periG), tractional retinal detachment (TRD), retinal folds (RF), and vitreous strands (VS) and was analyzed in 36 patients with UWF-SLO and 56 patients with CFP. Diagnostic tests were employed using the clinical examination as gold standard.

**Results** In total of the 56 OT eyes, granulomas were identified in 91.1% (51/56) of eyes, including postG in 46.4% (26/56) of eyes, periG in 41.1% (23/56) of eyes, and combined granulomas in 3.6% (2/56) of eyes. TRD, RF, and VS were found in 28.6% (16/56), 51.8% (29/56), and 83.9% (47/56) of patients, respectively. Although the specificities of the diagnosis in clinical features were similar by the diagnostic tests, the sensitivities of postG, periG, TRD, RF, and VS using UWF-SLO were 100%, 100%, 66.7%, 95%, and 81.8%, respectively, which were significantly higher those of CFP (72.2%, 31.3%, 11.1%, 55%, and 48.5%). Additionally, the extent of vitreous haze was milder graded by UWF-SLO compared to CFP ($p = 0.0099$).

**Conclusions** The diagnostic ability of UWF-SLO was superior to CFP using clinical examination as gold standard for the ascertainment of the characteristic manifestations of OT, especially for granulomas and RF.

## Introduction

Ocular toxocariasis (OT), first reported by Wilder in 1950 [1], is an ocular parasitosis caused by infection with *Toxocara canis* or *Toxocara cati* larvae, which are the most ubiquitous gastrointestinal helminths in dogs and cats. The incidence of OT is more prevalent in geographical areas where environmental factors and poor sanitary conditions favor the parasitism between human and animals. OT has been one of the main causes of pediatric infectious uveitis, especially in low or middle-income countries, where it is responsible for 17.7% of posterior uveitis in South America and 5.1% in São Paulo, Brazil [2]. In the last decade, several reports have shown an increasing prevalence of OT in China [3–5].

The spectrum of clinical features in OT is varies widely, the most common manifestations are peripheral inflammatory mass, posterior pole granuloma, and endophthalmitis [6]. It can include signs such as strabismus, band keratopathy, cataracts, cyclitic membrane, vitreous opacity, retinal folds (RF), retinal detachment, and epiretinal membranes, which often lead to severe visual impairment and even complete loss of vision. OT is mainly diagnosed clinically. Serological tests, such as

These authors contributed equally: Songshan Li, Limei Sun

**Supplementary information** The online version of this article (https://doi.org/10.1038/s41433-020-01332-w) contains supplementary material, which is available to authorized users.

✉ Xiaoyan Ding
dingxiaoyan@gzzoc.com

[1] State Key Laboratory of Ophthalmology, Zhongshan Ophthalmic Center, Sun Yat-sen University, Guangzhou, China

[2] Department of General Surgery, Peking Union Medical College Hospital, Chinese Academy of Medical Sciences and Peking Union Medical College, 100730 Beijing, China

enzyme-linked immunosorbent assay (ELISA) for the detection of serum antibodies against *Toxocara* larvae, provide evidence for *Toxocara* infection and may greatly support the process of diagnosis. However, since OT often develops in pediatric patients, ocular examination can be particularly challenging [5, 6]. Thus, the development of a fast, noninvasive diagnostic test that can be easily performed in pediatric populations is necessary for better detection and prompt diagnosis of OT.

Clinically, comprehensive mydriatic slit-lamp microscopy and fundus photography are essential for the diagnosis of OT. Conventional fundus photography (CFP) images with 20–50° fields of view are useful for documenting the location and effects of posterior granulomas in eyes with relatively clear media [7]. However, with a single field image, peripheral involvement may go undetected. With the development of ultra-wide-field (UWF) retinal imaging techniques, the ultra-wide-field scanning laser ophthalmoscopy (UWF-SLO) is now used widely in the diagnosis of retinal vascular diseases, such as retinal vein occlusion, diabetic retinopathy, vasculitis, and familial exudative vitreoretinopathy [8–11]. Furthermore, it has been used in newborns [12] and premature infants [13].

To date, the imaging features and diagnostic performance of UWF-SLO and CFP have not been compared in OT cases. Thus, the purpose of our study is to compare the imagological characteristics of OT between UWF-SLO and CFP, and to evaluate the potential diagnostic ability of UWF-SLO in this disease.

## Materials and methods

### Patients and study design

This cross-sectional study was conducted in Zhongshan Ophthalmic Center, Sun Yat-Sen University with the permission of the Institutional Review Board and adhered to the tenets of the Declaration of Helsinki. Written informed consent was obtained from all patients; in the case of children, informed consent was obtained from their parents or legal guardians. A total of 56 patients (40 males and 16 females) with unilateral OT were enrolled in this study between April 2017 and September 2019. We used clinical diagnosis as the gold standard. The inclusion criteria were as follows: (1) a clinical diagnosis of OT confirmed by IgG for *Toxocara* in serum or aqueous humor, and an increased Goldmann–Witmer coefficient (GWC) [14]; (2) either UWF-SLO or CFP was obtained. The exclusion criteria were as follows: (1) a history of congenital eye disease or positive family history of any ocular disease; (2) the presence of other diseases or evidence of any condition other than OT that could affect visual acuity or cause vitreous haze; and (3) severe opacity of the refractive media or incoordination such that neither UWF-SLO nor CFP could be obtained (seven patients were excluded due to the severe opacity of the refractive media, including four with severe cataract, one with band keratopathy, and two with seclusion pupillae; four patients were excluded due to the incoordination for the imaging).

All patients underwent a comprehensive ophthalmic examination, including measurement of best-corrected visual acuity (BCVA), intraocular pressure, slit-lamp biomicroscopy, and careful fundus examination by an experienced pediatric retina specialist (XD). The presence and location of granulomas (posterior, peripheral, or both), tractional retinal detachment (TRD), RF, and vitreous strands (VS) were recorded. Briefly, a granuloma is defined as a solid yellow or white mass located sub- or intraretinally, which was confirmed further by optical coherence tomography (OCT), ultrasound biomicroscopy (UBM), or ultrasonography B scan. TRD is defined as the detachment of the neurosensory retina due to traction from the granuloma or vitreous proliferation, which could be also visualized on a B scan. RF is defined as the presence of disorganized retinal layers extending from the optic disc to the peripheral retina. VS are defined as tree-like or laminated dense proliferative vitreal features as seen by fundoscopy. Representative examples of these clinical features are shown in Figs. 1–3.

### Image acquisition and analysis

As a novel imaging technique, UWF-SLO has been equipped in our hospital since 2018. Thus, in our study, 20 patients enrolled in 2017 received CFP only (Visucam 224, Carl Zeiss, Germany). After complete pupil dilation with 0.5% tropicamide, montaged CFP with the camera's built-in software was performed to cover as much as of the retina as possible. In 36 patients, who were enrolled after 2018, both CFP and UWF-SLO (Optomap 200Tx, Optos pls) were performed on the same day in an awakened state.

All images were interpreted by two independent blinded investigators separately (SL and LS). Any discrepancies in the data were resolved through reassessment and discussion with a third senior researcher (XD). The presence of major photographic biomarkers in OT was recorded and these included posterior or peripheral granuloma (periG), TRD, RF, and VS. Vitreous haze due to vitritis was evaluated based on UWF-SLO or CFP images separately. A previously reported method using a standardized photographic scale ranging from 0 to 4+ [15] was employed. Briefly, the

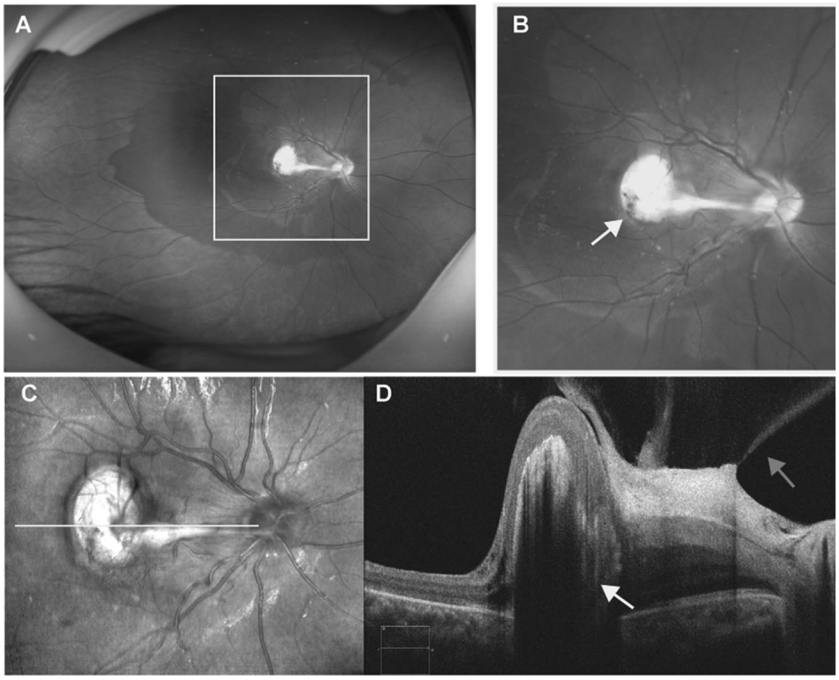


**Fig. 1 Presentations of ocular toxocariasis with posterior pole granuloma. A**, **B** A child (TX51) presenting with a posterior pole granuloma (yellow arrow) in macula, and vitreous strands (red arrow) around the optic disk. **C**, **D** Optical coherence tomography of the posterior pole granuloma (yellow arrow) and vitreous strands (red arrow) in the same patient.

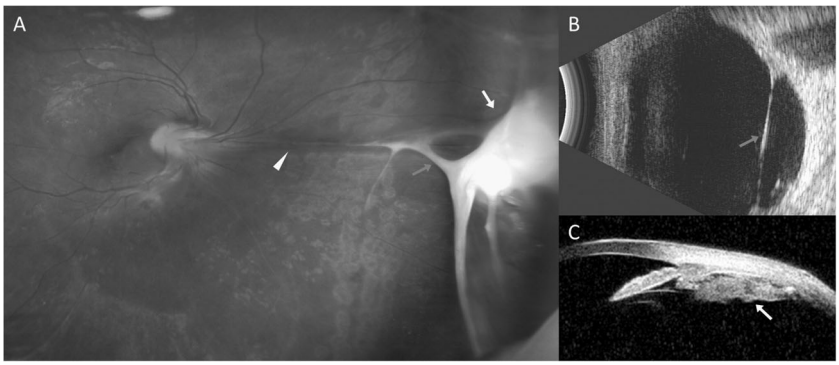


**Fig. 2 Presentations of ocular toxocariasis with peripheral granuloma. A** A UWF-SLO image of a peripheral granuloma (yellow arrow) with retinal folding (yellow arrowhead) and vitreous strands (red arrow) in a child (TX09). **B** B-scan ultrasound of vitreous strands (red arrow) between the optic disk and peripheral granuloma. **C** Ultrasound biomicroscopy of the peripheral granuloma (yellow arrow).

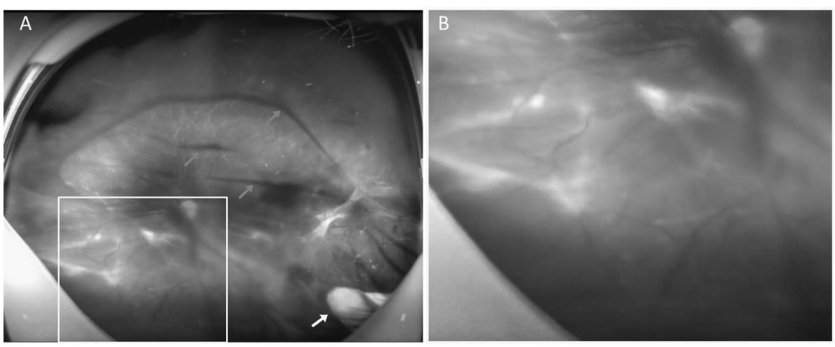


**Fig. 3 Presentation of tractional retinal detachment and vitreous strands in a patient with peripheral granuloma. A**, **B** UWF-SLO images of nasal tractional detachment (yellow box), vitreous strands (red arrow), and an inferior temporal peripheral granuloma (yellow arrow) in a child (TX62).

scale is as follows: 0, no evidence of any vitreous haze; 0.5+, slight blurring of the optic disc margins and/or loss of the nerve fiber layer reflex; 1+, mild blurring of the retinal vessels and optic nerve; 2+, moderate blurring of the optic nerve head; 3+, marked blurring of the optic nerve head; and 4+, optic nerve head not visible.

**Table 1** Demographic and clinical characteristics of patients ($n = 56$).

| | |
|---|---|
| Number of eyes (patients) | 56 (56) |
| Mean age ± SD (range, median), years | 9.68 ± 7.09 (1–40, median 7) |
| Male/female | 40/16 |
| OD/OS | 32/24 |
| BCVA (logMar) ± SD (range, median) | 1.60 ± 1.20 (0–5, median 1.6) |
| Number of patients with BCVA (logMar 0.4-0.0) (*n*, %) | 6 (10.7) |
| Mean intraocular fluid anti-Toxocara lgG titer ± SD (range, median) | 23.34 ± 15.52 (3.06–63.94, median 25.70) |
| Mean serum anti-Toxocara lgG titer ± SD (range, median) | 26.81 ± 12.67 (10.54–60.45, median 23.07) |
| Mean Goldmann–Witmer coefficient ± SD (range, median) | 149.95 ± 337.42 (5.23–1816.66, median 49.05) |

### Anti-*Toxocara* IgG ELISA test

Anti-Toxocara IgG titer were determined in serum or aqueous samples with the *T. canis* IgG ELISA kit (RE58721, IBL International, Inc., Germany), as the method reported by Wang et al. [16]. The value for specific IgG of serum samples higher than 11U was considered positive. Aqueous levels higher than the mean plus two standard deviations (SD) of values obtained in normal controls were considered to be positive. The GWC value exceeding three was considered as positive.

### Statistical analysis

Statistical analysis was performed using GraphPad Prism (GraphPad Software, CA, USA) or SPSS (version 16.0, SPSS Inc., Chicago, IL, USA). Comparisons of dichotomous data were performed with Pearson's chi-squared test (or Fisher's exact test when appropriate). Kappa analysis was performed to examine the intra- and interobserver agreement between two trained readers masked to the patient diagnosis and information. Diagnostic sensitivity, specificity, percentage agreement, and Youden index were calculated for each parameter. The level of agreement was determined by Cohen's $\kappa$-analysis. Kappa values were interpreted as follows: <0, poor agreement; 0–0.20, slight agreement; 0.21–0.40, fair agreement; 0.41–0.60, moderate agreement; 0.61–0.80, substantial agreement; and >0.80, almost perfect agreement. The level of significance was set at $p = 0.05$.

## Results

### Demographic and clinical characteristics

A total of 56 eyes from 56 patients with unilateral OT confirmed by serological/immunological test were enrolled in this study. Overall, 71.4% (40/56) of the patients were male and the mean age was 9.68 ± 7.09 years old (range 1–40, median 7). 89.3% (50/56) of patients were under 18 years old, while 10.7% (6/56) were adults at their first visit (Table 1).

In general, granulomas (posterior, peripheral, or combined) were found in 91.1% (51/56) of eyes. Posterior pole granuloma was found in 46.4% (26/56) of eyes, periG in 41.1% (23/56) of eyes, and combined granuloma in 3.6% (2/56) of eyes. An absence of granuloma was noted in 5.4% (3/56) of eyes with diffuse vitreous haze even after careful examination accompanied with multi-model imaging evaluation, which were diagnosed as endophthalmitis type. 3.6% (2/56) of eyes exhibited advanced proliferative retinal detachment in which the granuloma could not be distinguished. TRD was found in 28.6% (16/56) of eyes. RF and VS were detected in 51.8% (29/56) and 83.9% (47/56) of patients, respectively.

### Intra- and interobserver agreement in UWF-SLO and CFP image reading

Intra- and interobserver agreement with regard to describing the presence of major features, including postG, periG, TRD, RF, and VS, was demonstrated based on examination and multimodal imaging. When these five features were considered, the intra-observer agreements were almost perfect for both UWF-SLO ($\kappa = 0.986$, 0.944, 0.940, 0.986, and 0.903, respectively) and CFP interpretation ($\kappa = 0.924$, 0.983, 0.983, 0.944, and 0.924, respectively). The interobserver agreements were good to very good for UWF-SLO ($\kappa = 0.944$, 0.834, 0.840, 0.888, and 0.724, respectively). However, the interobserver agreements were only achieved moderate agreement for TRD by CFP ($\kappa = 0.563$). For postG detection, the interobserver agreement was lower for CFP compared to UWF-SLO ($\kappa = 0.944$ vs 0.649) (Table 2).

### Diagnostic tests in 36 eyes with UWF-SLO and CFP

To compare the diagnostic abilities of UWF-SLO and CFP, a diagnostic test was performed in 36 eyes using both

**Table 2** Interobserver agreement regarding the fundus characters in SLO and CFP.

| | | SLO ($n = 36$) | | | | | CFP ($n = 56$) | | | | |
|---|---|---|---|---|---|---|---|---|---|---|---|
| | Observer 1 | Observer 2 | | Agreement, % | Kappa (95% CI) | Strength of agreement | Observer 2 | | Agreement, % | Kappa (95% CI) | Strength of agreement |
| | | + | − | | | | + | − | | | |
| Posterior pole granuloma | + | 18 | 0 | 97.20 | 0.944 (0.837–1.000) | Very good | 15 | 2 | 83.93 | 0.649 (0.444–0.854) | Good |
| | − | 1 | 17 | | | | 7 | 32 | | | |
| Peripheral granuloma | + | 16 | 0 | 91.70 | 0.834 (0.657–1.000) | Very good | 9 | 1 | 94.64 | 0.824 (0.632–1.000) | Very good |
| | − | 3 | 17 | | | | 2 | 44 | | | |
| Tractional retinal detachment | + | 7 | 0 | 94.40 | 0.840 (0.627–1.000) | Very good | 5 | 3 | 89.29 | 0.563 (0.250–0.875) | Moderate |
| | − | 2 | 27 | | | | 3 | 45 | | | |
| Retinal fold | + | 19 | 0 | 94.40 | 0.888 (0.738–1.000) | Very good | 13 | 3 | 94.64 | 0.861 (0.709–1.000) | Very good |
| | − | 2 | 15 | | | | 0 | 40 | | | |
| Vitreous strands | + | 24 | 3 | 88.89 | 0.724 (0.473–0.975) | Good | 24 | 4 | 91.07 | 0.821 (0.673–0.970) | Very good |
| | − | 1 | 8 | | | | 1 | 27 | | | |

**Table 3** The detection rate of fundus characters in SLO and CFP.

| | SLO | CFP | $p$ |
|---|---|---|---|
| Posterior granuloma ($n = 18$) | 18 (100%) | 13 (72.2%) | 0.045[a] |
| Peripheral granuloma ($n = 16$) | 16 (100%) | 5 (31.3%) | <0.0001[a] |
| Tractional retinal detachment ($n = 9$) | 6 (66.7%) | 1 (11.1%) | 0.05[a] |
| Retinal folds ($n = 20$) | 19 (95%) | 11 (55%) | 0.0084[a] |
| Vitreous strands ($n = 33$) | 27 (81.8%) | 16 (48.5) | 0.0045 |

[a]Fisher test.

UWF-SLO and CFP. First, we compared the detection rate of the aforementioned five clinical features by UWF-SLO and CFP. According to the clinical findings, postG was detected in 18/36 OT eyes and periG was detected in 16/36 eyes. In the postG group, 100% (18/18) of granulomas were identified by UWF-SLO, while only 72.2% (13/18) were seen in CFP ($p = 0.045$). In the periG group, all (16/16) granulomas were detected by UWF-SLO, while only 31.3% (5/16) could be identified by CFP ($p < 0.0001$). TRD, RF, and VS were identified clinically in 9 (25.0%), 20 (55.5%), and 33 (91.7%) eyes. They were detected in 66.7% (6/9), 95.0% (19/20), and 81.8% (27/36) of eyes by UWF-SLO, which are statistically significantly higher than those by CFP: 11.1% (1/9), 55.0% (11/20), and 48.5% (16/36) ($p =$ 0.05, 0.0084, and 0.0045, respectively) (Table 3).

## Diagnostic sensitivity and specificity by UWF-SLO and CFP

Considering the high prevalence of these five features in OT, a diagnostic test was performed. By UWF-SLO, the detectivity of postG achieved perfect agreement ($\kappa = 1.0$) with a sensitivity of 100% and specificity of 100%. However, the detection rate by CFP was only moderate agreed (31/36 cases), with a $\kappa$ value of 0.722, sensitivity of 72.2%, and specificity of 100% ($p = 0.046$ for sensitivity and $p =$ 1.0 for specificity).

The detection of periG also achieved perfect agreement ($\kappa = 1.0$) with a sensitivity of 100% and specificity of 100% by UWF-SLO. By CFP, an agreement was achieved in 25/36 cases, with a $\kappa$ value of 0.313, sensitivity of 31.3%, and specificity of 100% ($p = 0.0001$ for sensitivity and $p = 1.0$ for specificity). In cases with PeriG, only 5/16 cases could be diagnosed by CFP (Fig. 4).

The detection of TRD by UWF-SLO achieved good agreement (32/36 cases) with a $\kappa$ value of 0.680, sensitivity of 66.7%, and specificity of 96.3%. A consensus was not reached in four cases. TRD was too subtle to be detected by UWF-SLO in three eyes and one eye with proliferative vitreous membrane was wrongly classified as having TRD. The agreement of TRD detection by CFP was very poor, with a $\kappa$ value of 0, sensitivity of 11.1%, and specificity of 88.9% ($p = 0.12$ for sensitivity and $p = 1.0$ for specificity).

The detection of RF achieved almost perfect agreement (35/36 cases) by UWF-SLO, with a $\kappa$ value of 0.944, sensitivity of 95.0%, and specificity of 100%. A consensus was not reached in only one patient. The agreement of RF detection in CFP was fair, with a $\kappa$ value of 0.464, sensitivity of 55.0%, and specificity of 93.8%. RF were detected by CFP in only 11/20 cases ($p = 0.0084$ for sensitivity and $p = 1.0$ for specificity).

The presence of VS was noted with good agreement by UWF-SLO (30/36 cases) with a $\kappa$ value of 0.659, sensitivity of 81.8%, and specificity of 100%. A consensus was not reached in six cases with VS. In CFP, only poor agreement was achieved (18/36 cases) with a $\kappa$ value of 0.087, sensitivity of 48.5%, and specificity of 66.7%. VS was not detectable by CFP in 17/33 cases and one patient presented with possible VS but without a typical manifestation on the B scan ($p = 0.009$ for sensitivity and $p = 1.0$ for specificity) (Table 4 and Fig. 4).

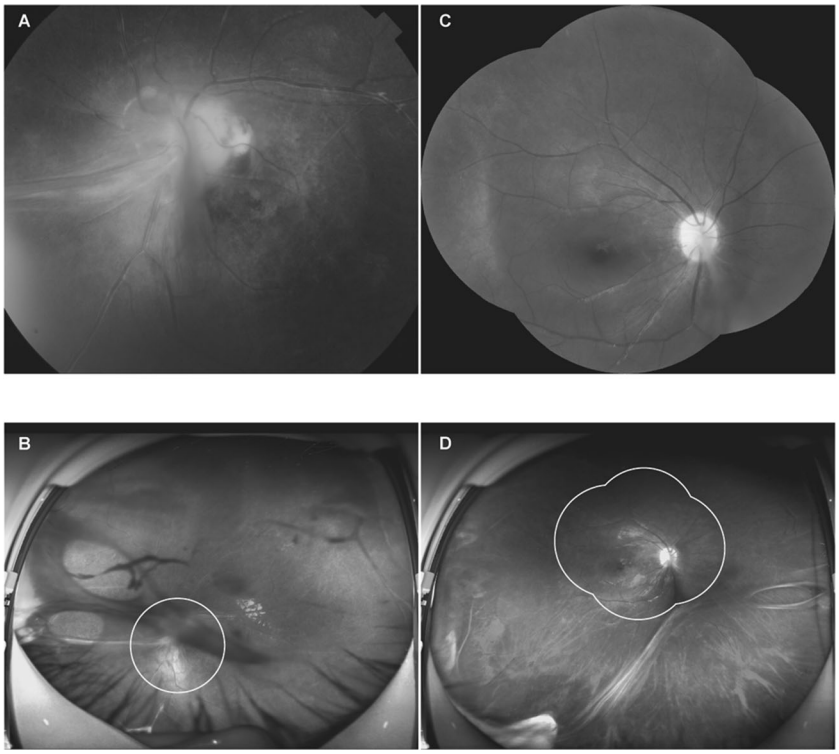


**Fig. 4 Comparisons between UWF-SLO images and conventional fundus photographs of two patients with ocular toxocariasis.** Conventional fundus photography (**A**) and UWF-SLO (**B**) was performed in a child (TX13) to cover as much of the retina as possible. The area corresponding to CFP was marked by yellow circle. Montaged conventional fundus photography (**C**) of a child (TX39) showed slight vitreous haze and barely visible fibrosis along the inferonasal and inferotemporal arcade. **D** UWF-SLO image clearly showed vitreous strands and an inferior temporal peripheral granuloma in the same patient.

## Comparison of vitreous haze grading between UWF-SLO and CFP

In 36 patients with both UWF-SLO and CFP images, the grade of vitreous haze was evaluated using the previously reported criteria. In CFP, 1 (2.8%), 7 (19.4%), 8 (22.2%), 6 (16.7%), 9 (25.0%), and 5 (13.9%) patients were graded 0, 0.5+, and 1+ to 4+ on the scale for vitreous haze, respectively. However, the grading of vitreous haze was significantly lower in UWF-SLO in the same patients with 1 (2.8%), 16 (44.4%), 3 (8.3%), 9 (25.0%), 6 (16.7%), and 1 (2.8%) patients graded as 0, 0.5, and 1+ to 4+, respectively ($p = 0.044$, chi-square test for trend) (Fig. 5) (Supplementary Table).

## Discussion

Because of diverse and occult clinical presentations, the diagnosis of OT is difficult. Granuloma is one of the features with the greatest diagnostic significance in OT. However, only 20–40% granuloma located in the posterior pole of the fundus [17]. In our study, periGs were observed in 41% of patients in the peripheral retina/far-peripheral retina, which is consistent with 43.7% reported by Sahu et al. [18]. In addition, most of the patients with OT are children with the mean age of onset being 7.5 years [19]. In our current study, the median age of onset was 7 years. Furthermore, vitreous opacity due to vitritis was presented in almost all OT patients and further increased the difficulty of diagnosis.

Recently, many attempts have been made to facilitate earlier diagnosis of OT using approaches such as ultrasonography, UBM, and OCT. In particular, ultrasonography was recently employed for OT diagnosis [20]. A solid, highly reflective mass attached to a multi-layered vitreous membrane is considered a characteristic manifestation of OT [3, 20]. However, the detection of this sign is greatly dependent on eyeball orientation and it is only present in a few OT patients with severe vitreous proliferation. UBM has been proven to be valuable in detecting periGs [20, 21], but it requires a plastic or silicone eyecup to hold a coupling medium. The contact nature of this instrument may make it impractical for many clinical scenarios. A subretinal or intraretinal mass on OCT was described in a patient with granuloma in the posterior pole [22]. Nevertheless, a clear refractive media is pivotal for high-quality OCT, which is extremely uncommon in OT patients. Hence, a simpler imaging technique is still required in clinical practice for the diagnosis, treatment, and follow-up of OT.

The last two decades saw the rapid development of UWF imaging, which has been used widely in retinal screening for rapid, single-frame photographic access to not only the posterior pole, but also the middle and far periphery. According to the Diabetic Retinopathy Clinical Research network, fundus photography with a field wider than 100° is considered to be UWF [23]. The 200° wide field of

**Table 4** Diagnostic performance of SLO and CFP for fundus characters.

| | SLO | | | | | CFP | | | | | |
|---|---|---|---|---|---|---|---|---|---|---|---|
| | Sensitivity, % | Specificity, % | Youden index | Kappa (95% CI) | Agreement | Sensitivity, % | Specificity, % | Youden index | Kappa (95% CI) | Agreement | *p* (sensitivity) | *p* (specificity) |
| Posterior granuloma | 100 | 100 | 1 | 1.0 (1.0–1.0) | Perfect | 72.2 | 100 | 0.722 | 0.722 (0.505–0.939) | Good | 0.046 | 1.0 |
| Peripheral granuloma | 100 | 100 | 1 | 1.0 (1.0–1.0) | Perfect | 31.3 | 100 | 0.313 | 0.313 (0.073–0.552) | Fair | 0.0001 | 1.0 |
| Tractional retinal detachment | 66.7 | 96.3 | 0.630 | 0.680 (0.392–0.968) | Good | 11.1 | 88.9 | 0 | 0 (−0.291 to 0.291) | Poor | 0.12 | 1.0 |
| Retinal fold | 95 | 100 | 0.95 | 0.944 (0.836–1.0) | Very good | 55 | 93.8 | 0.488 | 0.464 (0.209–0.720) | Moderate | 0.0084 | 1.0 |
| Vitreous strands | 81.8 | 100 | 0.818 | 0.659 (0.421–0.896) | Good | 48.5 | 66.7 | 0.152 | 0.087 (−0.126 to 0.214) | Poor | 0.009 | 1.0 |

UWF-SLO can provide coverage of 82% of the retina in adults. In contrast, only 15% of the retina can be visualized by CFP from a single 45° image [24, 25]. On account of its noncontact and tolerable nature in comparison with CFP, UWF-SLO has even been used to obtain high-quality images in infants [13]. This examination can be carried out swiftly and more conveniently in pediatric patients.

In our study, the UWF-SLO images provide a wide view of the retina, even in patients with massive vitreous haze or cataracts. The 200° wide-field image by UWF-SLO is beneficial for the detection of characteristic OT manifestations located in the peripheral retina, such as periG, TRD, and RF. The detection rates of granulomas were 100% for both posterior and periGs, with the diagnostic sensitivity and specificity also being 100%. Conversely, in CFP, only 72.2% of posterior granulomas and 31.3% of periGs could be detected. Because of the value of granulomas for the diagnosis of OT, UWF-SLO is highly recommended in patients who are suspected of having OT. UWF-SLO also exhibited good to very good agreement in diagnostic tests for TRD, RF, and VS. In contrast, the agreement of these three signs was only poor to moderate in CFP. In addition, UWF-SLO permitted better infiltration through the cloudy vitreous and lens because of the improved penetrability of lasers [26]. The grading of the vitreous haze in UWF-SLO was lower than CFP in 55.6% (20/36) of patients. These results may explain why UWF-SLO had a better detection rate for not only peripheral lesions, but also posterior granulomas. It is worth noting that CFP might be superior compared with UWF-SLO in quantifying the level of vitreous haze and monitoring the uveitis activity due to the ability of reflecting the actual vitreous situation. In addition, although superior diagnostic ability was proven in UWF-SLO compared with CFP for ascertainment several OT manifestations, the gold standard for OT diagnosis is still the clinical examination.

Our study included a moderately large population of OT patients diagnosed by serology/immunology and involved the analysis and comparison of the diagnostic value of UWF-SLO and CFP. Nevertheless, there remain several limitations. First, patients with clinical OT manifestations and negative *Toxocara* antibody were excluded from our study, which may induce the selection bias. Nevertheless, the test for *Toxocara* antibodies may not have high sensitivity, such that some OT patients may have been wrongly excluded. In addition, since most of the OT cases were young children who were often uncooperative, the detectivity may been reduced and image quality may be compromised. Lastly, the sample size in the current study was limited due to the rarity of OT, which makes it difficult to recruit a larger cohort. Further investigations with more cases in various cohorts are warranted to confirm our observations.

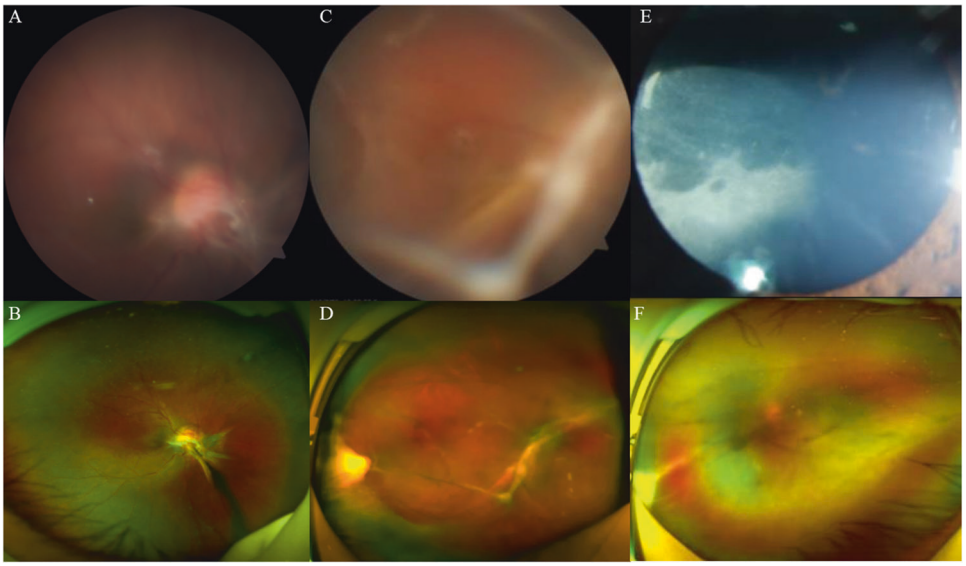


**Fig. 5 Differences in vitreous haze grading between conventional fundus photography and UWF-SLO in the same patient. A** Vitreous haze was graded of 2 in a child (TX69) on conventional fundus photography. **B** The vitreous haze in the same patient was graded of 0.5 by UWF-SLO image. **C** A vitreous haze was graded of 3 on conventional fundus photography and 2 on UWF-SLO in a patient (TX57) (**D**). **E** A child (TX40) with limited view of the retina because of a severe cataract in the right eye. **F** An UWF-SLO image showing the whole fundus and enabling diagnosis of the disease in the same case.

In conclusion, UWF-SLO demonstrated excellent diagnostic ability compared to CFP for ascertainment of the most common characteristic manifestations of OT, such as granulomas and RF.

## Summary

### What was known before

- The diagnosis of OT is based on the detection of characteristic features, like granuloma, which could be particularly challenging.

### What this study adds

- Ultra-wide-field scanning laser ophthalmoscopy (UWF-SLO) is a better imaging system for the ascertainment of the characteristic manifestations of OT compared with the conventional camera imaging (CFP), especially for pediatric patients.

**Acknowledgements** The authors thank all patients who participated in this study.

**Funding** Supported in part by grants from the Fundamental Research Funds of State Key Laboratory of Ophthalmology, research funds of Sun Yat-sen University (15ykjc22d; Guangzhou, Guangdong, China) (18zxxt73; Guangzhou, Guangdong, China), Science and technology program Guangdong, China (2016A020215096; Guangzhou, Guangdong, China) (2018A030310230; Guangzhou, Guangdong, China), and the grant from the National Natural Science Foundation of China (31800873). The sponsors and funding organizations had no role in the design or conduct of this research.

## Compliance with ethical standards

**Conflict of interest** The authors declare that they have no conflict of interest.

**Publisher's note** Springer Nature remains neutral with regard to jurisdictional claims in published maps and institutional affiliations.

## References

1. Rodman J, Pizzimenti J. In vivo diagnostic imaging of ocular toxocariasis. Clin Exp Optom. 2009;92:146–9.
2. Souto FMS, Giampietro BV, Takiuti JT, Campos LMA, Hirata CE, Yamamoto JH. Clinical features of paediatric uveitis at a tertiary referral centre in Sao Paulo, SP, Brazil. Br J Ophthalmol. 2018;0:1–5.
3. Liu Y, Zhang Q, Li J, Ji X, Xu Y, Zhao P. Clinical characteristics of pediatric patients with ocular toxocariasis in China. Ophthalmologica. 2016;235:97–105.
4. Zhang H-F, Wang W, Hua H-Y. Pediatric ocular toxocariasis in jiangsu province, Eastern China. Southeast Asian J tropical Med Public Health. 2015;46:8–14.
5. Zhou M, Chang Q, Gonzales JA, Chen Q, Zhang Y, Huang X, et al. Clinical characteristics of ocular toxocariasis in Eastern China. Graefes Arch Clin Exp Ophthalmol. 2012;250:1373–8.
6. Arevalo JF, Espinoza JV, Arevalo FA. Ocular toxocariasis. J Pediatr Ophthalmol Strabismus. 2013;50:76–86.
7. Campbell JP, Wilkinson CP. Imaging in the diagnosis and management of ocular toxocariasis. Int Ophthalmol Clin. 2012;52:145–53.
8. Lyu J, Zhang Q, Wang SY, Chen YY, Xu Y, Zhao PQ. Ultra-wide-field scanning laser ophthalmoscopy assists in the clinical detection and evaluation of asymptomatic early-stage familial exudative vitreoretinopathy. Graefes Arch Clin Exp Ophthalmol. 2017;255:39–47.
9. Sun JK, Aiello LP. The future of ultrawide field imaging for diabetic retinopathy: pondering the retinal periphery. JAMA Ophthalmol. 2016;134:247–8.
10. Prasad PS, Oliver SC, Coffee RE, Hubschman JP, Schwartz SD. Ultra wide-field angiographic characteristics of branch retinal and

hemicentral retinal vein occlusion. Ophthalmology. 2010;117:780–4.
11. Karampelas M, Sim DA, Chu C, Carreno E, Keane PA, Zarranz-Ventura J, et al. Quantitative analysis of peripheral vasculitis, ischemia, and vascular leakage in uveitis using ultra-widefield fluorescein angiography. Am J Ophthalmol. 2015;159:1161–8.1.
12. Magnusdottir V, Vehmeijer WB, Eliasdottir TS, Hardarson SH, Schalij-Delfos NE, Stefánsson E. Fundus imaging in newborn children with wide-field scanning laser ophthalmoscope. Acta Ophthalmol. 2017;95:842–4.
13. Fung TH, Muqit MM, Mordant DJ, Smith LM, Patel CK. Non-contact high-resolution ultra-wide-field oral fluorescein angiography in premature infants with retinopathy of prematurity. JAMA Ophthalmol. 2014;132:108–10.
14. Ma G, Holland CV, Wang T, Hofmann A, Fan C-K, Maizels RM, et al. Human toxocariasis. Lancet Infect Dis. 2018;18:e14–24.
15. Lowder C, Belfort R Jr., Lightman S, Foster CS, Robinson MR, Schiffman RM, et al. Dexamethasone intravitreal implant for noninfectious intermediate or posterior uveitis. Arch Ophthalmol. 2011;129:545–53.
16. Wang ZJ, Zhou M, Cao WJ, Ji J, Bi YW, Huang X, et al. Evaluation of the Goldmann-Witmer coefficient in the immunological diagnosis of ocular toxocariasis. Acta Trop. 2016;158:20–3.
17. Martínez-Pulgarín DF, Muñoz-Urbano M, Gomez-Suta LD, Delgado OM, Rodriguez-Morales AJ. Ocular toxocariasis: new diagnostic and therapeutic perspectives. Recent Pat Antiinfective Drug Discov. 2015;10:35–41.
18. Sahu ES, Pal B, Sharma T, Biswas J. Clinical profile, treatment, and visual outcome of ocular Toxocara in a tertiary eye care centre. Ocul Immunol Inflamm. 2018;26:753–9.
19. Taylor MR. The epidemiology of ocular toxocariasis. J Helminthol. 2001;75:109–18.
20. Liu J, Li S, Deng G, Yang W, Chen W, Lu H. Ultrasound biomicroscopic imaging in paediatric ocular toxocariasis. Br J Ophthalmol. 2017;101:1514–7.
21. Chen Q, Gu J, Jiang R, Zhou M, Chang Q. Role of ultrasound biomicroscopy in diagnosis of ocular toxocariasis. Br J Ophthalmol. 2018;102:642–6.
22. do LagoI A, AndradeI R, MuccioliI C, Belfort R Jr. Optical coherence tomography in presumed subretinal Toxocara granuloma: case report. Arq Bras Oftalmol. 2006;69:403–5.
23. Baker CW, Jiang Y, Stone T. Recent advancements in diabetic retinopathy treatment from the Diabetic Retinopathy Clinical Research Network. Curr Opin Ophthalmol. 2016;27:210–6.
24. Ghasemi Falavarjani K, Tsui I, Sadda SR. Ultra-wide-field imaging in diabetic retinopathy. Vis Res. 2017;139:187–90.
25. Cunningham ET Jr., Munk MR, Kiss S, Zierhut M. Ultra-wide-field imaging in uveitis. Ocul Immunol Inflamm. 2019;27:345–8.
26. Oishi A, Hidaka J, Yoshimura N. Quantification of the image obtained with a wide-field scanning ophthalmoscope. Investig Ophthalmol Vis Sci. 2014;55:2424–31.